FREQUENCY-DEPENDENT COUPLING BETWEEN RHYTHMICALLY ACTIVE NEURONS IN THE LEECH

ERIC PETERSON
Biological Laboratories, Harvard University, Cambridge, Massachusetts 02138

ABSTRACT The heart excitor (HE) cells, a set of rhythmically active motor neurons, drive the heartbeat of the medicinal leech. Their activity is gated by inhibitory input from a network of interneurons, but that influence may be modified locally by electrotonic coupling between the HE cells. In this paper I analyze that electrotonic coupling by applying direct current and alternating current signals, and compare the results with predictions based on linear cable theory. The electrotonic junction itself appears to be conventional, but because of the membrane properties of the HE cells, the coupling strength depends upon both the frequency and polarity of the signal and the phase of heartbeat cycle when the signal is applied.

GLOSSARY

R_m, resistance per unit area of membrane;
C_m, capacitance per unit area of membrane;
R_i, specific resistance of cytoplasm;
d, diameter of fiber;
r_m, membrane resistance per unit length of fiber;
c_m, membrane capacitance per unit length of fiber;
r_a, intracellular resistance per unit length of fiber;
i_a, intracellular axial current;
λ, cable space constant;
τ, membrane time constant;
T, time (t) normalized to units of τ (dimensionless);
W, angular frequency normalized to τ (dimensionless);
L, cable length (l) normalized to units of λ (dimensionless);
X, distance along the cable (x) normalized to λ (dimensionless);
G_0, conductance of the soma at $X = 0$;
G_L, conductance of the soma at $X = L$;
V, electrotonic potential.
List of symbols after Jack et al., 1975.

INTRODUCTION

There is now general agreement that synaptic inhibition is a major force shaping the output of rhythmic neural circuits in invertebrates (Roberts and Roberts, 1983). By contrast, excitation in the form of electrotonic coupling, although prevalent, often appears to make little direct contribution to pattern generation and in particular does not necessarily synchronize the activity of coupled neurons (Ort et al., 1974; Selverston et al., 1976; Thompson and Stent, 1976*c*). Even when its direct contribution appears to be small, coupling may nevertheless be important for proper pattern generation. For example, coupling between neurons that are active at different phases may provide presynaptic modulation (Thompson and Stent, 1976*c*; Nicholls and Wallace, 1978) and thus contribute indirectly to pattern generation. In addition, electrotonic junctions linking rhythmically active neurons may serve to equilibrate their membrane potential over time spans longer than that of individual cycles, and thereby ultimately balance the strengths of contraction of the different muscles involved in the behavior (Ort et al., 1974).

The neural circuit driving the heartbeat of the medicinal leech is a network of interneurons and motor neurons linked by inhibitory synapses and electrotonic junctions (Stent et al., 1979). The midbody musculature of the leech forms a relatively uniform tube (Fig. 1 *A*) containing two longitudinal blood vessels called heart tubes, and a ventral nerve cord that expands to form a bilaterally symmetrical ganglion in each segment. In the midbody each hemiganglion contains a heart excitor (HE) motor neuron that innervates the ipsilateral heart tube in that segment (Thompson and Stent, 1976*a*) (Fig. 1 *B*). A set of interneurons, the heart interneurons (HN cells), phasically inhibits the HE cells, imposing an activity schedule (Fig. 1 *C*) upon the HE cells and thereby producing coordinated constriction of the heart tubes. In addition, as considered in this paper and noted independently by others (L. P. Tolbert, personal communication), the two HE cells in a ganglion are electrotonically coupled. The functional significance of electrotonic coupling is uncertain, but coupling is strong enough so that it must be considered in any future quantitative description of the network.

Because the normal activity of the HE cells is cyclical, it is appropriate, and convenient analytically, to study their properties in the frequency domain by applying sinusoidal current signals. Frequency domain analysis has previously been used on a limited scale to study the transfer properties of electrotonically coupled neurons (Hagiwara et al., 1959; Levitan et al., 1970; DiCaprio et al., 1974; Getting, 1974), including the Retzius cells of the leech (Hagiwara and Morita, 1962; French and DiCaprio, 1975).

Dr. Peterson's present address is the Department of Biology, McGill University, 1205 Av. Docteur Penfield, Montreal H3A 1B1, Canada.

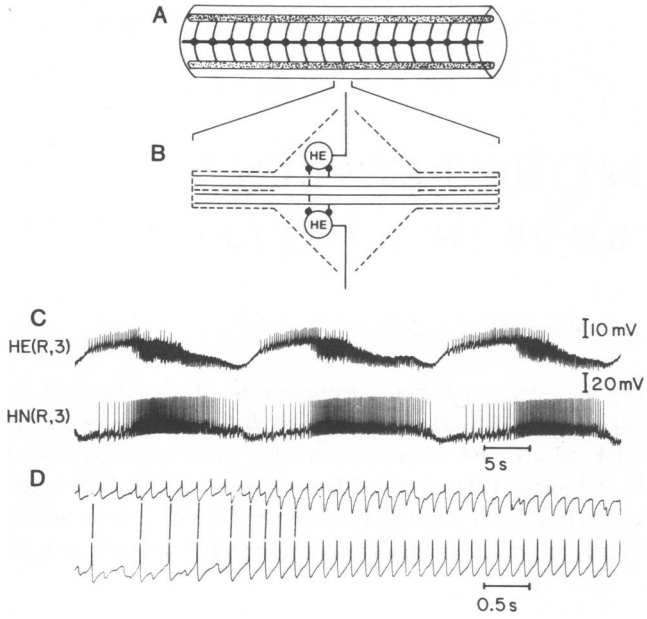

FIGURE 1 (*A*) Schematic of the segments that contain HE cells, including the segmental ganglia (●) linked with the lateral heart tubes (stippled) by segmental nerves. (*B*) The circuitry of a typical ganglion, greatly simplified. Each HE cell sends a single axon ipsilaterally. Axons of the intersegmental HE cells make inhibitory synapses (●) with the HE cells. There are at least five pairs of HN cells that synapse with HE cells, but for simplicity only two pairs are shown here. (For details see Stent et al., [1979].) (*C*) Simultaneous intercellular recordings from the HE cell on the right side of ganglion 3 (i.e., HE[R, 3]) and the HN(R, 3) cell, which synapses with the HE(R, 3) cell (Thompson and Stent, 1976*b*). (*D*) The recordings of *C* on a faster time scale. Each impulse in the HN cell precedes an inhibitory synaptic potential in the HE cell (events linked by solid lines).

METHODS

Leeches, *Hirudo medicinalis,* were obtained from a commercial supplier (Ricarimpex, 33980 Audenge, Gde, France). Single ganglia mounted using standard procedures were bathed in normal saline (Nicholls and Baylor, 1968), or in high Mg saline (normal saline with 40 mM MgCl replacing 60 mM of the NaCl). Microelectrodes filled with 4-M potassium acetate had resistance 35–60 M. Current signals were produced with a function generator and injected via an electrometer (Model 5, Getting Microelectrode Amplifier, Iowa City, IA) and stimulating microelectrode. A virtual ground probe monitored injected current. Data were recorded on tape then analyzed at low speed with either a storage oscilloscope or a chart recorder as appropriate. These recording procedures preserved all frequencies analyzed without attenuation.

Bode Plots

The frequency response of neurons is displayed by Bode plots (see D'Azzo and Houpis, 1966). The Bode plot includes two curves.

Frequency Transfer Curve. In this report the ordinate (measured in decibels) is either the voltage gain between two sites on a dendritic cable, or the alternating current (AC) input impedance relative to the direct current (DC) input resistance.

Phase Curve. The ordinate is either the phase angle between the voltage signals at two sites on the cable, or the phase angle between current and voltage signals, in degrees. The abscissa for both curves is the logarithm (base 10) of the frequency of the AC input signal.

As an illustration, a soma with no dendrites represents a simple lumped resistance and capacitance (Fig. 2 *A*, inset). As the input frequency approaches 0, the predicted frequency transfer curve (Fig. 2 *A*) approaches the DC input resistance. As the input frequency approaches infinity, the slope of the transfer curve approaches −6 dB for each doubling of the signal frequency. The intersection of the two asymptotes defines the cutoff frequency (f_c) at which the impedance is −3 dB relative to the DC resistance. The predicted phase curve (Fig. 2 *B*) approaches 0° as the input frequency approaches 0 and approaches −90° as the input frequency approaches infinity; the phase shift is −45° at the cutoff frequency.

CABLE EQUATIONS

The following assumptions are necessary to set the problem of the HE cells in a form that can be handled mathematically. Assumptions (*a–d*) follow those of Rall (1960); assumptions (*e–g*) are peculiar to the case of the HE cells. (*a*) The neuron is assumed to have an isopotential compartment including the soma that can be treated as a lumped resistance and capacitance. Given the structure of the HE cell (Shafer and Calabrese, 1981), the soma compartment probably includes the cell body and the large proximal portion of the main neurite. (*b*) The dendritic branches are assumed to be cylinders of uniform passive nerve membrane, having a resistance and a capacitance per unit area identical to that of the soma membrane. (*c*) The electrical current inside any fiber is assumed to flow axially through a resistance that is inversely proportional to the cross-sectional area of the fiber. (*d*) The extracellular space is assumed to be isopotential. (*e*) Dendrites are assumed to be of equivalent electrotonic length (Rall, 1962), and thus the set of dendrites can be treated as a single cable having the space constant of an individual dendrite. Almost all HE dendrites leave the main neurite medially and proceed with little branching toward the midline of the ganglion (Shafer and Calabrese, 1981). There is minor variation in the lengths of dendrites, but the assumption of

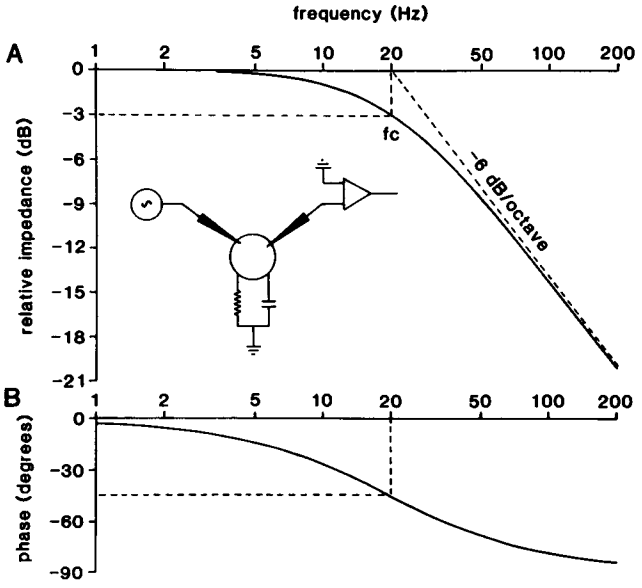

FIGURE 2 Frequency response predicted for a lumped resistance and capacitance (RC) network. (*A*) Frequency transfer curve. *Inset:* the stimulating and recording configuration for a resistance and capacitance arranged in parallel. *Ordinate:* the predicted impedance as a fraction of the DC impedance, measured in decibels. *Abscissa:* the frequency of the current signal, measured in hertz. The dashed reference lines are discussed in the text. (*B*) Phase curve. *Ordinate:* the predicted phase shift of the voltage response relative to the current signal, measured in degrees. *Abscissa:* as in *A*.

uniformity is reasonable given the HE anatomy. (*f*) Each dendritic process is assumed to end in an electrotonic junction with a dendritic process of the contralateral HE cell. Near the midline the processes branch and make contacts with the corresponding processes of the contralateral HE cell (L. P. Tolbert and R. L. Calabrese, unpublished results). Since serial sectioning has not been done, it is not certain that all dendrites form electrical junctions, but the great majority come into close proximity with terminals of the contralateral HE cell, as seen in light microscopy of whole mounts (Shafer and Calabrese, 1981; L. P. Tolbert and R. L. Calabrese, unpublished results). (*g*) The resistance of the electrotonic junction is assumed to be small relative to the total axial resistance of the dendrite leading to the junction. The sites of contact between HE cells are extensive (e.g., as long as 6 μm in sections) and over much of the area of contact one finds gap junctions (L. P. Tolbert and R. L. Calabrese, unpublished results) known to be sites of low resistance coupling between neurons (Pappas et al., 1971; Muller and Carbonetto, 1979). Therefore the equations will treat a pair of HE cells as a single cable terminated at each end by a lumped resistance and capacitance corresponding to the soma compartment (Fig. 3 *B*).

A comprehensive treatment of the mathematics of current spread in dendritic cables is available elsewhere (Jack et al., 1975). Here, that analysis and its extension to two experimental problems of interest is sketched. The basic equations relating voltage and current flow within a linear cable, normalized to the membrane time constant and space constant, are (for explanation of the symbols see Glossary)

$$\frac{\partial^2 V(X,T)}{\partial X^2} = \frac{\partial V(X,T)}{\partial T} + V(X,T) \tag{1}$$

$$i_a(X,T) = \frac{-1}{r_a\lambda}\frac{\partial V(X,T)}{\partial X}. \tag{2}$$

Laplace transforms (Jack et al., 1975) with respect to T are

$$\frac{\partial^2 \hat{V}(X,s)}{\partial X^2} - (s+1)\hat{V}(X,s) = 0 \tag{3}$$

$$\hat{i}_a(X,s) = \frac{-1}{r_a\lambda}\frac{\partial \hat{V}(X,s)}{\partial X} \tag{4}$$

(s, the transform of T, is a complex variable.)

Eq. 3 has a solution of the form

$$\hat{V}(X,s) = \hat{A}(s)\cosh\left(X\sqrt{s+1}\right) + \hat{B}(s)\sinh\left(X\sqrt{s+1}\right). \tag{5}$$

$\hat{A}(s)$ and $\hat{B}(s)$ will depend upon conditions at the boundaries, which in the present case will be the HE somata at the two ends of the cable, $X = 0$ and $X = L$. The two sets of experiments treated in detail later can be represented as follows.

Case 1

The voltage signal is generated in the soma at $X = 0$, then transferred to the soma at $X = L$. If the boundary condition at $X = 0$, is a specified voltage signal $\hat{V}(0,s)$, then trivially

$$\hat{A}(s) = \hat{V}(0,s). \tag{6}$$

At $X = L$ the current flow in the cable Eq. 4 must equal that across the soma membrane, which is given by

$$i_a(L,T) = G_L V(L,T) + G_L\frac{\partial V(L,T)}{\partial T}. \tag{7}$$

Upon Laplace transformation Eq. 7 becomes

$$\hat{i}_a(L,s) = (s+1)G_L\hat{V}(L,s). \tag{8}$$

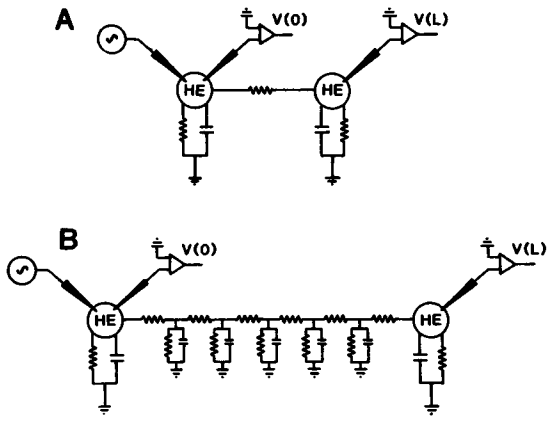

FIGURE 3 Alternative models for electrotonic coupling. (*A*) The somata are assumed to be linked by a simple resistance. If axial resistance were localized at the junction this model would apply. (*B*) The somata are assumed to be linked by a leaky cable having uniformly distributed axial resistance. (This uniform distribution is depicted as five discrete compartments.)

Therefore, equating Eqs. 4 and 8 and rearranging

$$\frac{\partial \hat{V}(L,s)}{\partial L} = -r_a\lambda(s+1)G_L\hat{V}(L,s), \tag{9}$$

but from Eq. 3

$$\frac{\partial \hat{V}(L,s)}{\partial L} = \sqrt{s+1} \cdot \left[\hat{A}(s)\sinh\left(L\sqrt{s+1}\right) + \hat{B}(s)\cosh\left(L\sqrt{s+1}\right)\right]. \tag{10}$$

Equating Eqs. 9 and 10 to get an expression for $\hat{B}(s)$, substituting this expression along with that for $\hat{A}(s)$ obtained in Eq. 6, into Eq. 3, then rearranging yields the solution to Eq. 3.

$$\frac{\hat{V}(L,s)}{\hat{V}(0,s)} = \frac{1}{\cosh\left(L\sqrt{s+1}\right) + G_L r_a\lambda\sqrt{s+1}\sinh\left(L\sqrt{s+1}\right)}. \tag{11}$$

That solution, evaluated at L, with jW substituted for s ($j = \sqrt{-1}$) is the predicted frequency response function of the cable (Jack and Redman, 1971).

The only unknown is the constant $G_L r_a\lambda$, which can be estimated from the DC coupling coefficient between the two somata $[\hat{V}(L,0)/\hat{V}(0,0)]$ after rearranging Eq. 11

$$K = G_L r_a\lambda = \frac{\dfrac{\hat{V}(0,0)}{\hat{V}(L,0)} - \cosh(L)}{\sinh(L)}. \tag{12}$$

Since the DC coupling coefficient is measurable, upon substitution of Eq. 12 into Eq. 11, the solution of Eq. 11 becomes an expression in the variable, W, and the single parameter, L.

Case 2: Input Impedance of an HE Soma

In this case a specified current signal is injected into the soma at $X = 0$. It is sufficient to consider the case where the signal is a delta function, and hence its Laplace transform with respect to T, $\hat{I}(s)$ is constant. Of course

Eqs. 3 and 4 still apply as does Eq. 8 since the boundary condition at $X = L$ is the same as in Case 1. At $X = 0$, $\hat{V}(0, s) = \hat{A}(s)$ and therefore

$$\hat{i}_a(0, s) = \hat{I}(s) - (s + 1)G_0\hat{A}(s), \tag{13}$$

but from Eq. 4 it is also true that

$$\hat{i}_a(0, s) = \frac{-\hat{B}(s)\sqrt{s + 1}}{r_a\lambda}. \tag{14}$$

In Eqs. 5 and 11, and the combination of Eqs. 13 and 14, there are three equations in three unknown functions of s: $\hat{A}(s)$, $\hat{B}(s)$, and $\hat{V}(L, s)$; and therefore a solution in terms of $\hat{A}(s)$ can be obtained directly. The required function specifying the input impedance of the soma at $X = 0$ is simply $\hat{A}(s)/\hat{I}(s)$, or

$$\hat{Z}(s) = \frac{r_a\lambda}{(s + 1)} \cdot [\sqrt{s + 1}\sinh(L\sqrt{s + 1})]/\{\cosh(L\sqrt{s + 1}) + K\sqrt{s + 1}\sinh(L\sqrt{s + 1}) - [1/\cosh(L\sqrt{s + 1}) + K\sqrt{s + 1}\sinh(L\sqrt{s + 1})]\}. \tag{15}$$

The constant, $r_a\lambda$, can be determined by measuring the input impedance at DC $[\hat{Z}(0)]$ then evaluating

$$r_a\lambda = \frac{\hat{Z}(0)}{\sinh(L)} \cdot \left[\cosh(L) + K\sinh(L) - \frac{1}{\cosh(L) + K\sinh(L)}\right]. \tag{16}$$

Numerical Evaluation

The complex-valued expressions for cosh and sinh were evaluated by summation of the first 25 terms of the Taylor series

$$\cosh(L\sqrt{jW + 1}) = \sum_{k=0}^{\infty} \frac{(L\sqrt{jW + 1})^{2k}}{(2k)!} \tag{17}$$

$$\sqrt{jW + 1}\sinh(L\sqrt{jW + 1}) = \sum_{k=0}^{\infty} \frac{L^{2k+1}\sqrt{jW + 1}^{2k+2}}{(2k + 1)!}. \tag{18}$$

RESULTS

The model derived in the preceding section represents the HE cells as a pair of somata linked by a leaky dendritic cable (Fig. 3 *B*). Here the model is tested by injecting known current signals into one HE soma and measuring the resulting voltage fluctuations. The qualitative features of the response to 6 and 60 Hz sinusoidal signals (Fig. 4) are as follows. (*a*) The response of the injected cell is asymmetrical, implying that input impedance falls with depolarization. (This asymmetry, which will be shown to be independent of frequency, will be termed rectification, which in neurophysiological usage refers to a voltage-dependent change in resistance.) (*b*) The input impedance of the injected cell decreases as frequency increases. (*c*) The HE cells are electrotonically coupled. (*d*) The coupling strength decreases as frequency increases. The elements of this complex response are analyzed in the following sections.

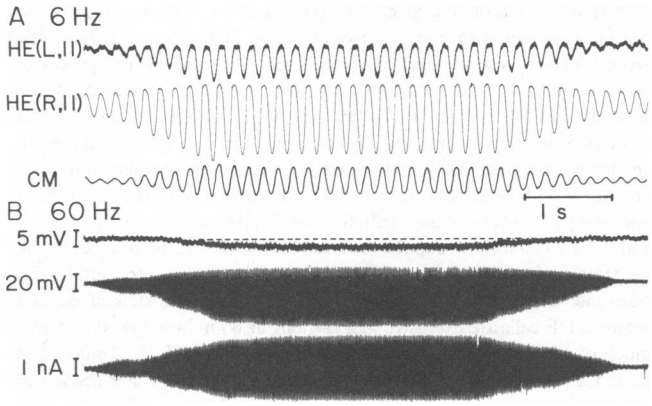

FIGURE 4 Response to sinusoidal current signals. *A* and *B* were obtained in successive trials with the pair of HE cells in ganglion 11. In both frames the top trace is an intracellular recording of the HE cell on the left side of the ganglion, the middle trace is an intracellular recording of the HE cell on the right side of the ganglion. The current monitor (CM) shows the current injected into HE(R, 11). Scale bars in *B* refer to traces in both frames. (*A*) 6-Hz current signal. (The current monitor trace was retouched.) (*B*) 60-Hz current signal. The broken line above the voltage trace of cell HE(L, 11) extrapolates the prestimulus resting potential.

Steady-State Properties of the HE Cells

In normal saline, HE cells alternate between firing spontaneously and receiving synaptic inhibition (Fig. 1 *C*), and thus it is difficult to measure their steady-state properties. Square pulses of current, 1-s long, were applied during intervals between bursts of inhibition, and voltage deflections were measured relative to a reference line 5-mV above the undershoots of the action potentials occurring at the peak of the active phase. For hyperpolarizing pulses that were strong enough to block spiking, the voltage-current (*VI*) relationship (Fig. 5 *A*) was linear with a mean slope resistance (dV/dI) of 47.9 MΩ ($n = 10$). In the range more positive than the spike threshold, the slope resistance fell sharply to ~15–20 MΩ and decreased further for increased depolarization. This precipitous drop in slope resistance upon depolarization is not characteristic of leech motor neurons in general (Stuart, 1970; Zipser, 1979).

More precise measurements are possible in high Mg saline, which blocks spontaneous activity and chemical synaptic transmission in the leech (Nicholls and Purves, 1970). In high Mg saline the resting potential of an HE cell was ~15 mV lower than the reference potential in normal saline, but the *VI* relationship was similar. In the hyperpolarizing region the mean slope resistance was 62 MΩ ($n = 6$) (Fig. 5 *B*), and in the depolarizing range it eventually fell to ~15 MΩ, although impulses generally were not seen. In both normal and high Mg saline there was a drop in slope resistance as the membrane was shifted to potentials more positive than −45 mV. Thus although

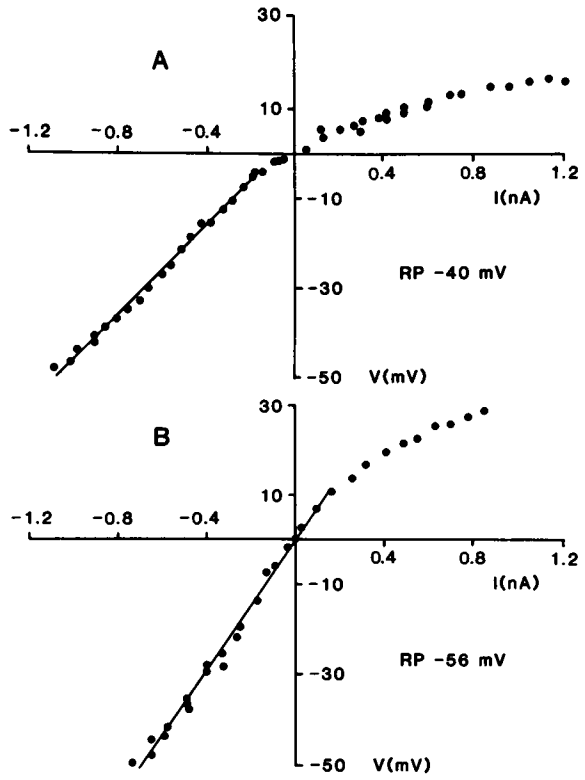

FIGURE 5 Steady-state properties of an HE cell. (*A*) Normal saline. Current pulses of 1-s duration were delivered, and the steady-state voltage deflection (V) measured. The reference potential (see text) was −40 mV. (The regression lines in *A* and *B* were fitted by eye.) (*B*) High Mg saline. The resting potential was −56 mV.

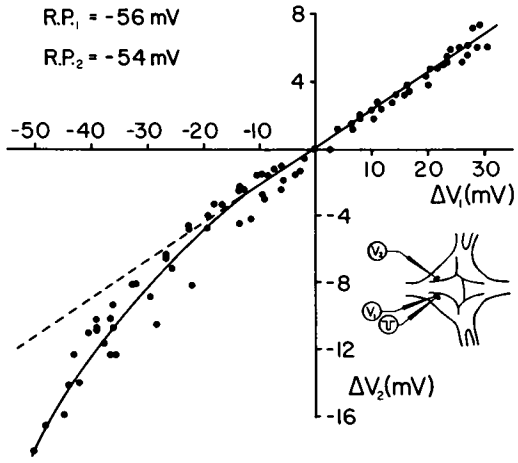

FIGURE 6 Steady-state electrotonic coupling between the HE cells (High Mg saline). Current pulses were applied to one HE soma and the steady-state response of each cell was measured. The voltage deflection of the second cell is plotted as a function of the voltage deflection of the first cell. The straight line was fitted by eye to the points within the range −20 mV < $V1$ < 20 mV. The deviation from linearity for large hyperpolarizing currents is unexplained.

high Mg saline hyperpolarizes an HE cell and increases its input resistance slightly, it does not substantially change its current-voltage relationship.

The steady-state coupling coefficient is the ratio $V(L)/V(0)$, where $V(0)$ is the voltage deflection of the HE cell injected with current and $V(L)$ that of the other HE cell. In high Mg saline this coefficient ranged from 0.10 to 0.30 (Fig. 6) (mean = 0.17; n = 4) and was independent of polarity for moderate currents. Since the drop in slope resistance (Fig. 5) was not correlated with a decrease in the DC coupling coefficient between the two somata (Fig. 6), it evidently reflects a change in the soma compartment rather than a change in the dendritic cable. As discussed below, in normal saline the coupling coefficient fluctuates during the burst cycle reflecting changes in the membrane properties of the HE cells.

Membrane Time Constant

Rall (1959, 1960) noted that the charging curve for current step applied to a neuron reflects two time constants, one caused by charging the soma membrane, τ, and the other caused by axial flow of current into the dendrites. Shunting by electrotonic coupling to other neurons further complicates the measurement of τ (Getting, 1974). However because τ is generally longer than the time constants of the competing processes, it can be estimated from the tail of the charging curve (Jack and Redman, 1971; Getting, 1974). τ for an HE soma could also be estimated from the time course of discrete inhibitory postsynaptic potentials (IPSPs), a method that was preferable since it required the insertion of only one microelectrode, and therefore caused little damage. For example, large, isolated IPSPs in an HE cell in the fourth segmental ganglion decay with a single time constant (Fig. 7) assumed to be τ. (In theory [Rall, 1962] currents injected via synapses will produce charging curves with a single time constant if the synapses are uniformly distributed on the target cell. Because the HN(3) and HE(4) cells overlap extensively [Shafer and Calabrese, 1981], it is possible that synaptic

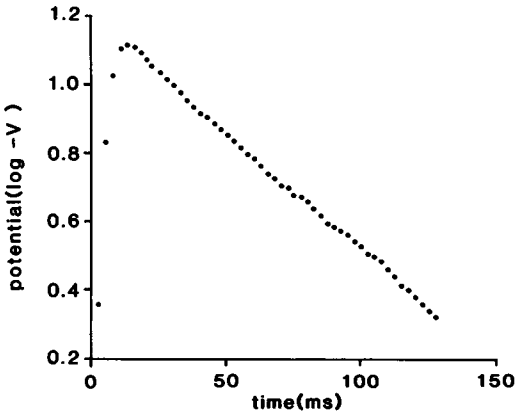

FIGURE 7 The time course of IPSPs in an HE cell. *Ordinate:* the log of V, the voltage deflection from rest. *Abscissa:* the time in milliseconds from the onset of the IPSP. The data are mean values for three isolated IPSPs produced in an HE(4) cell by impulses of the ipsilateral HN(3) cell (Thompson and Stent, 1976*b*). The time constant of this cell was estimated to be 60 ms.

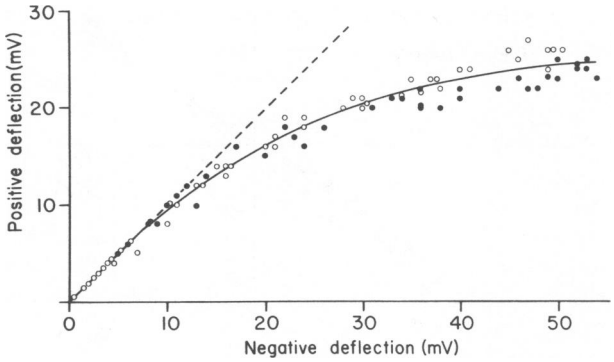

FIGURE 8 Rectification is independent of frequency. A series of sinusoidal current signals was applied to an HE(11) cell. *Ordinate:* the maximum deflection of the membrane potential of the HE cell in the depolarizing direction. *Abscissa:* the maximum deflection in the hyperpolarizing direction. ●, frequencies <10 Hz. ○, frequencies >10 Hz. On the dashed line (---) positive and negative deflections are equal.

input is widely distributed, as it is for other leech neurons [DeRiemer and Macagno, 1981], and that this explains the simple kinetics of the IPSP.) Estimates for τ obtained either from the tails of charging curves, or from IPSP decay profiles were in the range 55–75 ms.

Frequency Response of an HE Soma

Ideally the frequency response of the HE cells would be measured by generating sinusoidal voltage signals in one soma and measuring their attenuation in the other, however, owing to rectification by the soma membrane (Fig. 5), the voltage signals produced by current injection are not pure sinusoids (Fig. 4). Fig. 8 shows positive voltage deflection as a function of negative voltage deflection for a wide range of frequencies and amplitudes of stimulus currents. For larger deflections there was a clear asymmetry, but the values for high and low frequencies (contrasting symbols) formed a single cloud. Thus, the general shape of the voltage signal is essentially independent of frequency for a given amplitude, and by holding the amplitude of a current signal constant, one can manipulate frequency as an independent variable.

Fig. 9 shows the frequency response of an HE soma injected with sinusoidal current signals, together with the curve predicted from Eq. 15 for experimentally determined values of τ, the DC coupling coefficient, and the L parameter (see Fig. 10). For comparison in Fig. 9 the curves predicted if the HE soma behaved as a lumped RC network (Fig. 2) are also plotted. In general the theoretical curves predicted by the two models both fit the experimental results fairly well, although the fit of the curve predicted by the cable model was slightly better. (Slight discrepancies between the experimental curve and the curve predicted by the cable model are in the direction expected if some dendrites were not electrotonically coupled to processes of the contralateral HE cell.) In summary

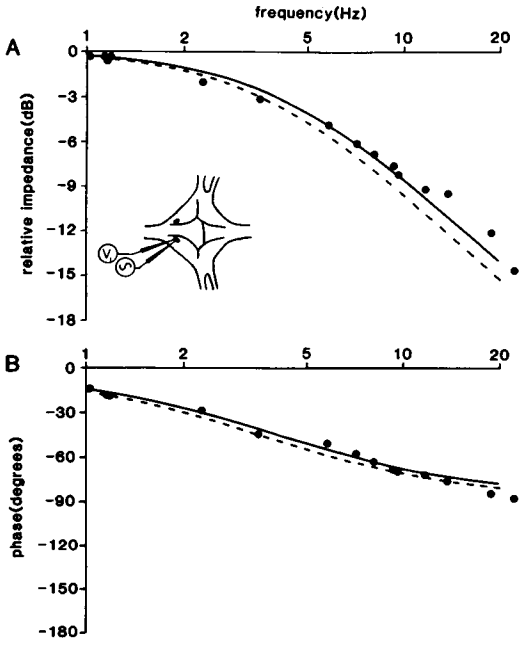

FIGURE 9 Input impedance as a function of frequency, (*A*) Frequency transfer curve for current signals injected into an HE soma. *Ordinate:* the input impedance of the HE cell relative to the DC input resistance, in decibels. (*B*) Phase curve. *Ordinate:* the phase of the voltage response relative to the current signal. *Abscissa:* in both cases is the frequency of the applied current signal. τ was 45 ms. The solid curves are those predicted by the cable model (Fig. 3 *B*); the broken curves are those predicted by the lumped RC model (Fig. 2).

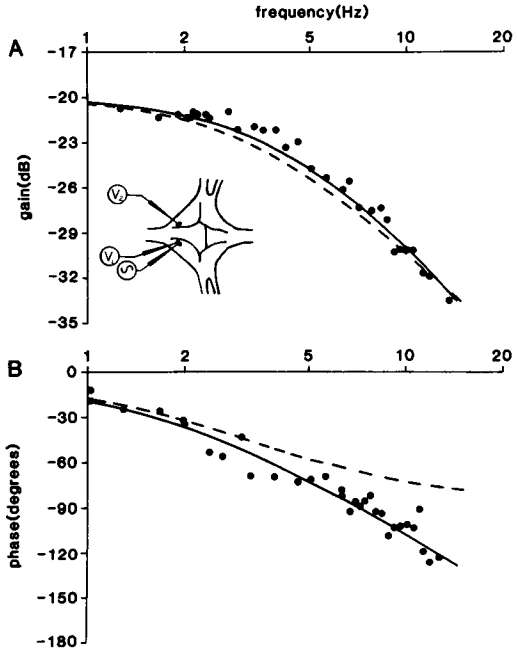

FIGURE 10 Electrotonic coupling as a function of frequency. (*A*) Frequency transfer curve for signals sent between the two HE somata. *Ordinate:* the gain in decibels. (*B*) Phase curve. *Ordinate:* the phase shift of the signal as it spreads from one soma to the other. *Abscissa* (for both curves): the frequency of the applied current signal. For this pair of cells τ was 50 ms and the DC gain was 0.1. The solid curves are those predicted by the cable model (Fig. 3 *B*); the broken curves are those predicted by the localized resistance model (Fig. 3 *A*).

the experimental results are in good agreement with the cable model (Fig. 3 *B*), but they do not exclude competing models since the response is evidently dominated by the RC properties of the injected soma.

AC Coupling Between HE Somata

Fig. 10 plots the gain and phase angle between the voltage signals in the two HE somata as a function of frequency for current signals sufficient to produce a 60-mV (peak-to-peak) oscillation in the injected cell. Given the values for v and the DC coupling coefficient measured above, Eq. 11 predicts the frequency response for any chosen value of the parameter L (which is the effective separation of the two somata in space constants). L was varied until Eq. 11 produced a good fit to the experimental results. For the range of parameters obtained, the shape of the predicted phase curve was particularly sensitive to variation in L. For four HE pairs examined in detail and two pairs for which partial data were available, theoretical curves for L = 1.0–1.4 gave the best fit to the experimental curves (Fig. 10).

The element coupling two neurons has traditionally been treated as a simple resistance (Fig. 3 *A*) (Bennett, 1966). Since a cable with an infinitely long space constant is a simple axial resistance, that model is described by the limit of Eq. 11 as λ approaches infinity.

$$L \to 0$$

and

$$G_L r_a \lambda \sqrt{s+1} \sinh (L\sqrt{s+1}) \to G_L r_a \left(\frac{l}{L}\right) \sqrt{s+1}\,(L\sqrt{s+1})$$

therefore Eq. 11 reduces to

$$\hat{V}(s) = \frac{1}{1 + G_L r_a l (s+1)}. \tag{19}$$

The frequency transfer curve and the phase curve predicted by the simple resistance model are plotted for comparison in Fig. 10. Although the fit of the predicted frequency transfer curve is tolerable (but not as good as that of the cable model), the fit of the phase curve is poor. At all frequencies this model seriously underestimates the phase lag, and more significantly, this model predicts that the phase lag at high frequency should be asymptotic to 90°, whereas the measured phase lags clearly exceed that value. Thus the processes linking the two HE somata behave as a cable with continuous axial resistance (Fig. 3 *B*) rather than as a simple resistor (Fig. 3 *A*).

Filtering of Complex Signals

The processes of the HE cell preferentially attenuate not only higher frequency pure signals, but also higher frequency components of a complex signal. For example, owing to rectification, the oscillation induced by a 60-Hz current signal (Fig. 4) is the superposition of 60-Hz fundamental, higher frequency harmonics, and a 15-mV hyperpolarizing DC component. The 60 Hz and higher components are filtered out during passage to the other HE cell since they are far above the cutoff frequency (Fig. 10), leaving only the DC component remaining. Since the cells in Fig. 4 had a steady-state coupling coefficient of ~20%, the 15-mV shift in the HE(R) soma showed up as a 3-mV shift in the HE(L) soma. Similar but less pronounced effects are seen at 6 Hz (Fig. 4).

DISCUSSION

HE Cells are Electrotonically Coupled

By physiological tests the HE cells are electrotonically coupled, since currents pass from one soma to the other under conditions that suppress chemical synaptic transmission (Fig. 4). Nevertheless, the pair has properties that imply a more complicated relationship than a link via a conventional electrotonic junction. First, in normal saline hyperpolarizing potentials pass between the HE somata with much less attenuation than do depolarizing potentials, mimicking the "double rectification" reported for the T cells of the leech (Baylor and Nicholls, 1969). Second, the frequency transfer properties of the HE pair deviate from predictions for two somata linked by a simple coupling resistance (Fig. 10).

It is now clear that current flows between some T cells indirectly, via serial synapses with coupling interneurons (Muller, 1979), and that this relationship could easily account for double rectification (Baylor and Nicholls, 1969) and complicated frequency transfer properties. In the case of the HE cells, however, this possibility appears unlikely because as anatomical studies show (L. P. Tolbert and R. L. Calabrese, unpublished results) HE cells make direct contact and form gap junctions. It could be argued that there is a parallel pathway involving coupling neurons, but as discussed in the following section, there is no need to seek complicated explanations for the observed features of coupling between the HE cells.

Passive Properties of the HE Cells Affect Coupling

The apparent double rectification shown by the junction between the HE cells can be explained without attributing any rectifying properties to the junction itself. From Eq. 12 the DC coupling coefficient is

$$\frac{V(L,0)}{V(0,0)} = \frac{1}{\cosh (L) + G_L r_a \lambda \sinh (L)}, \tag{20}$$

where the signal is being transferred from 0 to L. Since all terms are positive for $L > 0$, as the slope conductance of the soma G_L increases, the coupling coefficient decreases. When an HE cell is in its active phase, its G_L depends critically upon the polarity of the applied current, being far

higher for depolarization than for hyperpolarization (Fig. 5 *A*). Hence it follows directly that the measured coupling coefficient would be smaller for depolarizing signals than for hyperpolarizing signals. When the HE cell at *L* is hyperpolarized beyond the inflection point of the *VI* curve, then its membrane becomes nonrectifying for small signals, and in turn the coupling coefficient measured for signals transferred from the other HE cell is independent of polarity (Fig. 6).

Although the frequency response of the junction between the HE cells deviates from the predictions of the traditional model for electrotonic coupling (Fig. 3 *A*), it agrees with an equally plausible model in which the two somata are linked by a leaky cable (Figs. 3 *B* and 10). In a normally cycling HE cell impulses and synaptic potentials occur at ~10 per second, and therefore generate frequency components equal to or higher than 10 Hz. Because this is well beyond the cutoff frequency for transfer, it is understandable that they produce no matching events in the contralateral HE soma. Thus, the strong rectification by the HE membrane accounts for the functional asymmetry of electrotonic coupling, and cable properties of the dendrites explain the deviation of the frequency transfer function from prediction.

Function of Electrotonic Coupling

In the intact nervous system the two HE cells in a given ganglion have a characteristic phase relationship to one another ranging from approximately in phase for ganglia at the rostral and caudal ends of the nerve cord to as much as 180° out-of-phase in some midbody ganglia (Calabrese and Peterson, 1983). Yet, each pair of HE cells, regardless of its location, is electrotonically coupled, arguing that coupling may have only slight importance for pattern generation.

In assessing the role of coupling, it is important to realize that its strength will be strongly phase dependent. That is, under normal conditions an HE cell alternates between a depolarized, active phase and a hyperpolarized, silent phase. That oscillation has a peak-to-peak amplitude of 10–20 mV around a mean of ~−45 mV. Since the membrane slope resistance of an HE cell decreases from ~50 MΩ to ~15 MΩ as the membrane potential becomes more positive than −45 mV (Fig. 5 *A*), the cell has a low slope resistance during the active phase and a high slope resistance during the silent phase. As discussed above, signals spreading from one HE cell across the dendritic cable to the second HE cell are attenuated by a factor inversely proportional to the slope resistance of the second HE cell. Low frequency fluctuation of the membrane potential in the first cell will therefore strongly influence the second cell when the second cell is in the silent phase, but have negligible effect when the second cell is in the active phase. It is possible that coupling, with its phase dependency, is important for fine tuning the pattern imposed by synaptic inhibition. Alternatively, as noted in the Introduction, coupling may simply serve to equilibrate the membrane potentials of two HE cells over longer time spans and thereby equalize the strength of constriction of the heart muscle on the two sides of the segment.

Cable Properties of Leech Neurons

The main neurites of two HE cells are separated by 200–300 μm (Shafer and Calabrese, 1981). Traced along the irregular path taken by a dendrite, the cables linking the two neurites are ~350-μm long and 0.75 μm in diameter (L. P. Tolbert, personal communication). Based on the analysis presented in this paper, such a cable is 1.0–1.4 space constants long. For comparison, leech S cells (Frank et al., 1975; Muller and Carbonetto, 1979) in adjacent ganglia are directly coupled by linear pathway including the axon of one S cell, an electrical junction, and the axon of the other S cell. At 10 μm in diameter the S axon should have a space constant ~3.6 times that of a 0.75-μm HE dendrite, or ~1,300 μm, other parameters being equal. In fact, the coupling coefficient between neighboring S cells is 0.1 (Frank et al., 1975), yielding an estimate of 2,200 μm for the space constant of the S fiber. Not surprisingly there is some discrepancy between the measured space constant of the S fiber and that extrapolated from the HE cell results, but the two values are certainly within the same range.

The coupling between the Retzius cells of the leech (Hagiwara and Morita, 1962; Eckert, 1963) has been analyzed with sinusoidal input signals by French and DiCaprio (1975). Their results fit a model in which the Retzius cells were represented as a pair of lumped resistances and capacitances linked by a simple resistance (Fig. 3 *B*). They considered an alternative model in which the pair of Retzius cells was represented as a leaky cable sealed at both ends. The predicted frequency response of this second model was at odds with the experimental results, and therefore the hypothesis that the cable properties of the dendrites alone produced the frequency dependence of the electrotonic coupling was rejected. Recently Chapman and Yang (1982) reexamined this problem and concluded that the coupling between the Retzius cells is well described by a cable model similar to the model presented in this paper (Fig. 3 *B*) (but formulated independently). The result suggests that HE cell coupling and Retzius cell coupling may have a common basis.

I thank L. P. Tolbert and R. L. Calabrese for discussion and permission to cite unpublished data.

This work was supported by a National Institutes of Health grant 1 R01 NS15101-01 to R. L. Calabrese.

Received for publication 30 September 1982 and in final form 5 March 1983.

REFERENCES

Baylor, D. A., and J. G. Nicholls. 1969. Chemical and electrical synaptic connexions between cutaneous mechanoreceptor neurones in the central nervous system of the leech. *J. Physiol. (Lond.).* 203:591–609.

Bennett, M. V. L. 1966. Physiology of electrotonic junctions. *Ann. N.Y. Acad. Sci.* 137:509–539.

Chapman, K. M. and J. Yang. 1982. Estimation of specific membrane and cable properties of leech Retzius cell electrotonic coupling. *Soc. Neurosci. Abstr.* 8:685.

D'Azzo, J. J., and C. H. Houpis. 1966. Feedback Control System Analysis and Synthesis. McGraw-Hill, Inc., New York. 824.

DeRiemer, S. A., and E. R. Macagno. 1981. Light microscopic analysis of contacts between pairs of identified leech neurons with combined use of horseradish-peroxidase and Lucifer yellow. *J. Neurosci.* 1:650–657.

DiCaprio, R. A., A. S. French, and E. J. Sanders. 1974. Dynamic properties of electrotonic coupling between cells of early *Xenopus* embryos. *Biophys J.* 14:387–411

Eckert, R. 1963. Electrical interaction of paired ganglion cells in the leech. *J. Gen. Physiol.* 46:573–587.

Frank, E., J. K. S. Jansen, and E. Rinvik. 1975. A multisomatic axon in the central nervous system of the leech. *J. Comp. Neurol.* 159:1–13.

French, A. S., and R. A. DiCaprio. 1975. The dynamic electrical behaviour of the electrotonic junction between Retzius cells in the leech. *Biol. Cybern.* 17:129–135.

Getting, P. A. 1974. Modification of neuron properties by electrotonic synapses. I. Input resistance, time constant, and integration. *J. Neurophysiol. (Bethesda).* 37:846–857.

Hagiwara, S., and H. Morita. 1962. Electrotonic transmission between two nerve cells in leech ganglion. *J. Neurophysiol. (Bethesda).* 25:721–731.

Hagiwara, S., A. Watanabe, and N. Saito. 1959. Potential changes in syncytial neurons of lobster cardiac ganglion. *J. Neurophysiol. (Bethesda).* 22:554–572

Jack, J. J. B., D. Noble, and R. W. Tsien. 1975. Electric Current Flow in Excitable Cells. Clarendon Press, Oxford, 502.

Jack, J. J. B., and S. J. Redman. 1971. An electrical description of the motoneurone, and its application to the analysis of synaptic potentials. *J. Physiol. (Lond.).* 215:321–352.

Levitan, H., L. Tauc, and J. P. Segundo. 1970. Electrical transmission among neurons in the buccal ganglion of a mollusc, *Navanax inermis, J. Gen. Physiol.* 55:484–496.

Muller, K. J. 1979. Synapses between neurones in the central nervous system of the leech. *Biol. Rev. Camb. Philos. Soc.* 54:99–134.

Muller, K. J., and S. T. Carbonetto. 1979. The morphological and physiological properties of a regenerating synapse in the C.N.S. of the leech. *J. Comp. Neurol.* 185:485–516.

Nicholls, J. G., and D. A. Baylor. 1968. Specific modalities and receptive fields of sensory neurons in the central nervous system of the leech. *J. Neurophysiol. (Bethesda).* 31:740–756.

Nicholls, J. G., and D. Purves. 1970. Monosynaptic chemical and electrical connexions between sensory and motor cells in the central nervous system of the leech. *J. Physiol. (Lond.).* 209:647–667.

Nicholls, J., and B. G. Wallace. 1978. Modulation of transmission at an inhibitory synapse in the central nervous of the leech. *J. Physiol. (Lond.).* 281:157–170.

Ort, C. A., W. B. Kristan, Jr., and G. S. Stent. 1974. Neuronal control of swimming in the medicinal leech. II. Identification and connections of motor neurons. *J. Comp. Physiol.* 94:121–154.

Pappas, G. D., Y. Asada, and M. V. L. Bennett. 1971. Morphological correlates of increased coupling resistance at an electrotonic synapse. *J. Cell Biol.* 49:173–188.

Rall, W. 1959. Branching dendritic trees and motoneuron membrane resistivity. *Exp. Neurol.* 1:491–527.

Rall, W. 1960. Membrane potential transients and membrane time constants of motoneurons. *Exp. Neurol.* 2:503–532.

Rall, W. 1962. Theory of physiological properties of dendrites. *Ann. N.Y. Acad. Sci.* 96:1071–1092.

Roberts, B. L., and A. Roberts. editors. 1983. Neural Basis of Rhythmic Movement. *Symp. Soc. Exp. Biol.* 37:404.

Selverston, A. I., D. F. Russell, J. P. Miller, and D. G. King. 1976. The stomatogastric nervous system: structure and function of a small neural network. *Prog. Neurobiol. (Oxf.).* 7:215–290.

Shafer, M. S., and R. L. Calabrese. 1981. Similarities and differences in the structure of segmentally homologous neurons that control the hearts in the leech, *Hirudo medicinalis. Cell Tissue Res.* 214:137–153.

Stent, G. S., W. J. Thompson, and R. L. Calabrese. 1979. Neural control of heartbeat in the leech and in some other invertebrates. *Physiol. Rev.* 59:163–176.

Stuart, A. E. 1970. Physiological and morphological properties of motoneurones in the central nervous system of the leech. *J. Physiol. (Lond.).* 209:627–646.

Thompson, W. J., and G. S. Stent. 1976*a*. Neuronal control of heartbeat in the medicinal leech. I. Generation of the vascular constriction rhythm by heart motor neurons. *J. Comp. Physiol.* 111:261–279.

Thompson, W. J., and G. S. Stent. 1976*b*. Neuronal control of heartbeat in the medicinal leech. II. Intersegmental coordination of heart motor neuron activity by heart interneurons. *J. Comp. Physiol.* 111:281–307.

Thompson, W. J., and G. S. Stent. 1976*c*. Neuronal control of heartbeat in the medicinal leech. III. Synaptic relations of the heart interneurons. *J. Comp. Physiol.* 111:309–333.

Zipser, B. 1979. Voltage-modulated membrane resistance in coupled leech neurons. *J. Neurophysiol. (Bethesda).* 42:465–475.